Chapter 6. AC and DC electrical conductivity and magnetic properties of $Co_{0.65}Zn_{0.35}Fe_{2-x}Mo_xO_4$ (x=0.0, 0.1 and 0.2) ferrites.

6.1 Introduction

As of late ferrimagnetic materials, i.e., generally ferrites, are innovatively and modernly most vital material because of their eminent magnetic and electrical behaviors. Likewise ferrites are presently utilized as the most essential constituent to build multiferroic composites [57]. Both ferroelectric and ferromagnetic ordering exhibits in multiferroic materials in a single phase [196]. Because of this captivating behaviors, the multiferroic materials are utilized to construct high density memory gadget where the information can be composed or perused in both the way, i.e., electrically and magnetically or the other way around [197]. The multiferroic materials likewise display magneto-electric impact in which the electrical behaviors may be fluctuated by applying externl magnetic field [81].

Among a few sorts of ferrites, Cobalt ferrite is generally critical. It has some prominent behaviors like low dielectric and magnetic loss, high resistivity, high dielectric constant, low eddy current, moderate saturation magnetization, chemical stability and low assembling cost and so on [202] making the material to a great degree valuable for flexible applications in various fields like magnetic recording, transducer, microwave electronics,

resonator, waveguides, magnetic coolant, satellite communication, magnetic switches, ferrofluids, controlled drug delivery, MRI (magnetic resonance imaging) and cancer thermotherapy and so forth [67, 114, 127, 135, 140]. The ferrites are the insulators with high Curie temperature (T_C) magnetic having non-zero magnetic moment with spin-dependent band gaps which might be utilized as a part of spintronics and spin-caloritronics [137]. It have inverse spinel crystal structure having chemical formula $CoFe_2O_4$. A shocking actuality is that the fractional substitution of Zn-ion on the A-site of the CFO astoundingly increments the saturation magnetization [8]. The techniques for preparation, sintering temperature and duration, substituents, grain size and so on assume a huge part to tune the magnetic and electrical behaviors of ferrites [67]. There are a few kinds of preparation techniques like ceramic method, sol-gel, hydrothermal, co-precipitation and so forth [119]. Among these, ceramic (solid state reaction) technique is reasonable to get ready polycrystalline Mo substituted Co-Zn ferrite in A-site of the inverse spinel.

A few invetigators have explored the effect of various doping on the magnetic and electrical behaviors of mixed ferrites. Nongjai *et al*. [127] have explored Indium substituted Co-ferrite and showed the diminishing of saturation magnetization and improve of electrical behaviors because of Indium substitution. The correlation between the magnetic and electrical behaviors close to Curie temperature is reported by Pradhan *et al*. [137]. Khandekar *et al*. [119] studied the impact of calcination temperature on structural and electrical properties of CFO. Meaz *et al*. [107] explored the role of Ti substitution on Co-Zn ferrite and noticed the diminishing in conductivity. The conduction process was clarified based on small polaron hopping mechanism. Cobalt ferrite nanoparticles had been

synthesized by Gopalan *et al*. [130]. The semiconducting character of Co-ferrite nanoparticles have been found. The small polaron tunneling theory was observed to be appropriate to clarify the dispersion of its ac conductivity. Albeit numerous studies have been completed by various research bunches far and wide however to the best of our insight, the detail electrical transport (AC and DC conductivity) and magnetic properties of Mo doped Co-Zn ferrites have not been accounted for yet.

In this chapter, we have exhibited the detail study on electrical transport (AC and DC conductivity) and magnetic properties of CZMO ferrite. The temperature and frequency variation of AC conductivity of all the polycrystalline samples has been investigated in detail. The activation energy of each sample in both paramagnetic and ferrimagnetic region have been assessed. The temperature reliance of magnetization and real part of permeability [$\mu = \mu_0(1 + \chi)$] at various frequency have also been contemplated in detail.

6.2 AC conductivity

6.2.1 Frequency dependence

The ac conductivity of a ferrite sample may be computed using the accompanying expression [116]

$$\sigma_{ac} = \varepsilon_0 \varepsilon' \omega \, tan \, \delta \qquad (6.1)$$

where tanδ displays the dielectric tangent loss, may be written as

$$tan \, \delta = {\varepsilon''}/_{\varepsilon'} \qquad (6.2)$$

Hence $\sigma_{ac} = \varepsilon_0 \, \omega \, \varepsilon''$ (6.3)

where ε_0 is permittivity in free space, ε′ and ε″ represents the real and imaginary part of dielectric constant respectively and the angular frequency of ac field is ω. The frequency reliance of ac conductivity for Mo doped Co-Zn ferrite is depicted in Fig. 6.1(a)-(c).

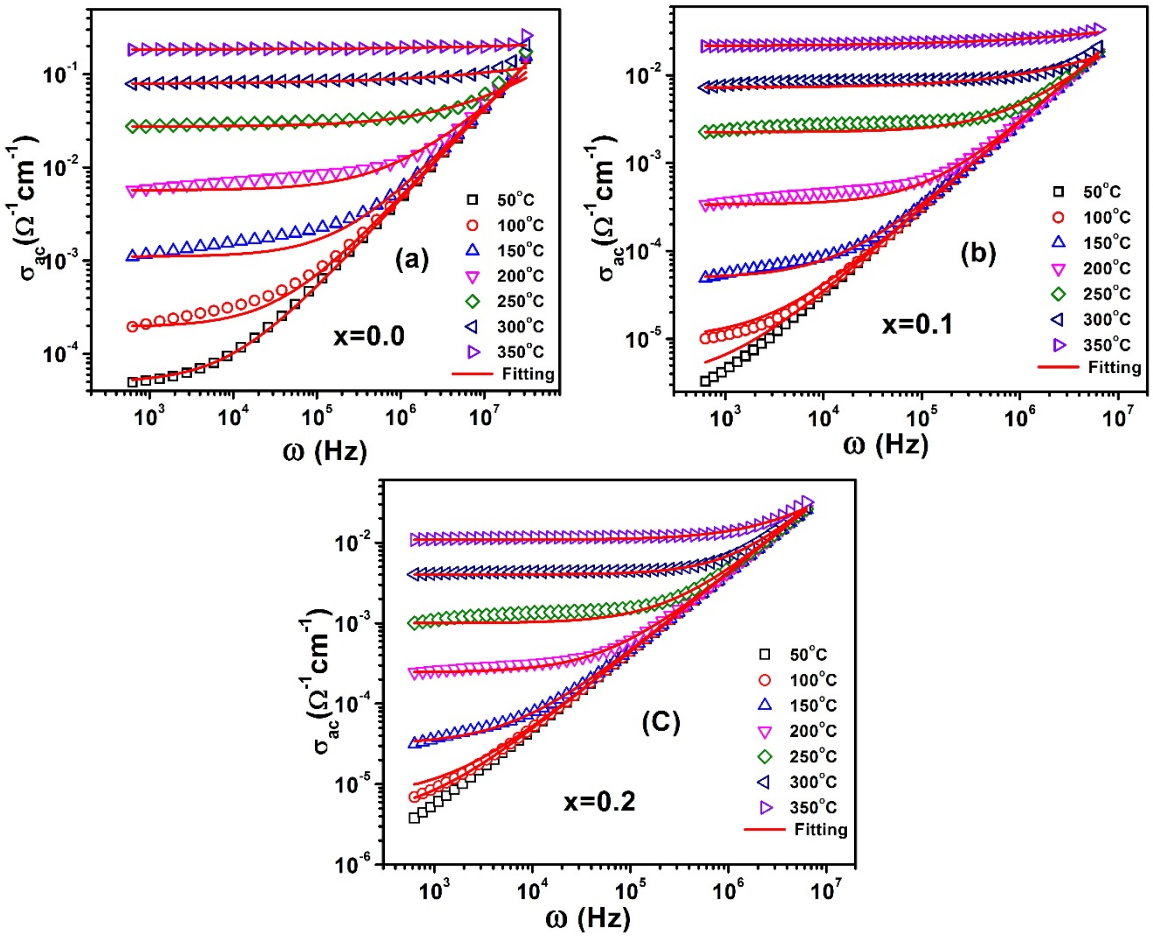

Fig. 6.1. (a)-(c) The variation of ac conductivity with frequency for CZMO for x=0.0, 0.1 and 0.2.

It is noticed that in σ_{ac} vs. f plots, there are two domains. The ac conductivity is frequency independent at low frequency domain and when the frequency rising up, at a

particular frequency the ac conductivity begins to increase rapidly with frequency. This specific frequency, at which σ_{ac} begins to raise, is called hopping frequency (ω_P). The plateau at lower frequency is the result of dc conductivity contribution while, the higher frequency dispersion is because of ac conductivity. Each curves comply with the Jonscher's single power law [113], may be illustrated as

$$\sigma_{ac} = \sigma_{dc} + A(T)\omega^n \qquad (6.4)$$

where σ_{dc} represent the frequency free dc conductivity, A(T) is the pre-factor which is temperature reliant with unit of conductivity and the temperature reliant unit less frequency exponent is *n*. The primary term relates to the drift mobility of the free charge, which prevail at low frequency and second term compares to the dielectric relaxation of the bound charge, which prevail at high frequency [107]. The solid lines in σ_{ac} vs. f curves are tastefully fitted as indicated by the power law. Every conductivity parameters, i.e., σ_{dc}, A(T) and n are estimated from the fitted data and recorded in Table 6.1. The absolute temperature reliant of n and A(T) with is outlined in Fig. 6.2.

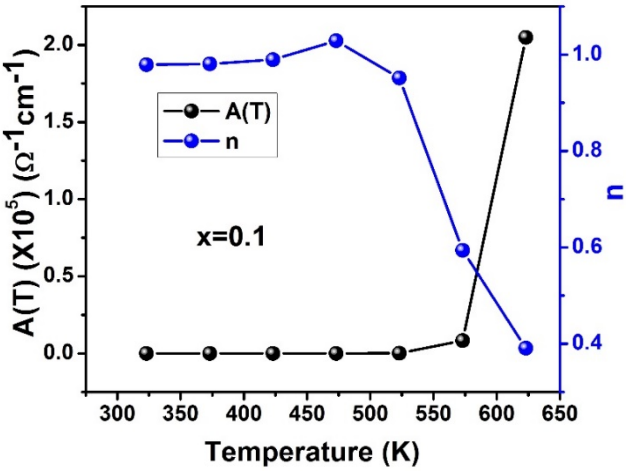

Fig. 6.2. Temperature dependence of conductivity pre-factor 'A(T)' and frequency exponent 'n' of $Co_{0.65}Zn_{0.35}Fe_{1.9}Mo_{0.1}O_4$.

Table 6.1. The ac conductivity parameters estimated from Jonscher's plot.

Temperature (K)	Parameters	Composition (x)		
		0.0	0.1	0.2
323	σ_{dc} ($\Omega^{-1}cm^{-1}$)	4.93E-5	3.286E-6	3.77E-6
	A(T) ($\Omega^{-1}cm^{-1}$)	7.04E-9	3.86E-9	5.39E-9
	n	0.9677	0.9789	0.9816
373	σ_{dc}($\Omega^{-1}cm^{-1}$)	1.948E-4	1E-5	6.92E-6
	A(T) ($\Omega^{-1}cm^{-1}$)	8.3E-9	3.8E-9	5.41E-9
	n	0.959	0.9808	0.98165
423	σ_{dc}($\Omega^{-1}cm^{-1}$)	0.001	`4.9E-5	3.135E-5
	A(T) ($\Omega^{-1}cm^{-1}$)	1.123E-8	3.32E-9	5.36E-9
	n	0.94	0.9896	0.9823
473	σ_{dc}($\Omega^{-1}cm^{-1}$)	0.0057	3.374E-4	2.44E-4
	A(T) ($\Omega^{-1}cm^{-1}$)	9.28E-8	1.789E-9	3.42E-9
	n	0.8041	1.029	1.01
523	σ_{dc}($\Omega^{-1}cm^{-1}$)	0.0274	0.00225	0.001
	A(T) ($\Omega^{-1}cm^{-1}$)	9.53E-7	4.73E-9	2.28E-9
	n	0.6433	0.9515	1.03
573	σ_{dc}($\Omega^{-1}cm^{-1}$)	0.0787	0.0072	0.004
	A(T) ($\Omega^{-1}cm^{-1}$)	7.02E-5	8.31E-7	4.06E-10
	n	0.3655	0.594	1.14
623	σ_{dc}($\Omega^{-1}cm^{-1}$)	0.1835	0.021	0.01
	A(T) ($\Omega^{-1}cm^{-1}$)	1.68E-4	2.05E-5	1.27E-8
	n	0.282	0.391	0.8979

It has been observed that n diminishes with temperature while A(T) demonstrates the contrary patterns. With increment in T, A(T) is relatively steady up to 570 K and after that all of a sudden starts to increase.

A few hypothetical theories have been proposed to correspond the conduction process of the ac conductivity. In quantum mechanical tunneling theory (QMT), n is temperature independent. On the off chance that n is diminishing with temperature, it achieves a base esteem and again increments with temperature. At that point, this compares

to overlapping large polaron tunneling theory (OLPT). In correlated barrier hopping model (CBH), n diminishes with temperature [124].

In our present investigation, the temperature reliance of n propose that the conduction is because of correlated barrier hopping (CBH) process illustrated as [128]

$$n = 1 - \frac{6k_BT}{W_H + k_BT\ln(\omega\tau_0)} \qquad (6.5)$$

where k_B is the Boltzmann constant, the absolute temperature is T, W_H represents the barrier height, the angular frequency is ω and the relaxation time is τ_0. The ac conductivity as indicated by CBH theory is

$$\sigma(\omega) = \frac{\pi^3}{24}[N(E_F)]^2\varepsilon\varepsilon_0\omega R_\omega^6 \qquad (6.6)$$

where $N(E_F)$ represents the density of state at Fermi level, dielectric constant is ε, ε_0 is permittivity in free space and R_ω shows the distance of hopping.

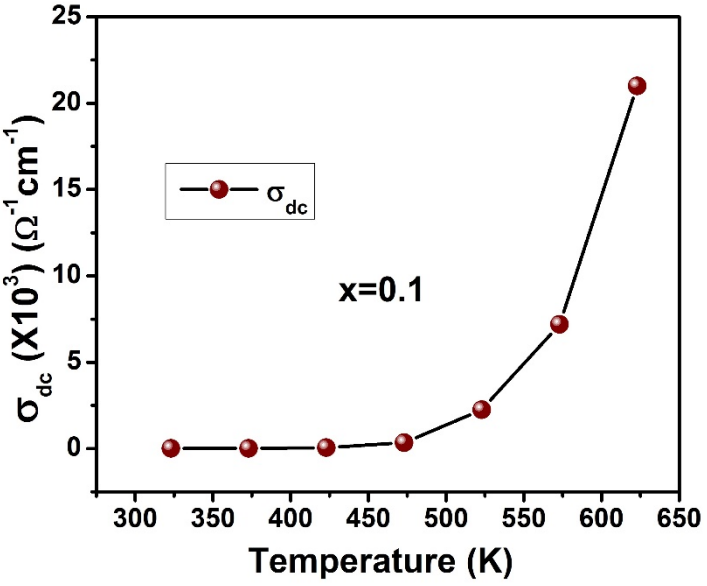

Fig. 6.3. The variation of dc conductivity with temperature for x=0.1.

Fig. 6.3 demonstrates the variation of dc conductivity with temperature uncovering that the dc conductivity increments exponentially with temperature obeying the Arrhenius condition.

The electrical conductivity in Mo substituted Co-Zn ferrite may be clarified based on Verwey-de Boer mechanism [225], in which the electron exchange include between particles of similar component display in excess of one valance state which are arbitrarily situated over different crystallographic lattice sites. A fractional reduction of Fe^{3+} to Fe^{2+} can occur at a specific temperature. The development of Fe^{2+} ion is because of the dissipation of Zn ions at the time of sintering procedure. Co^{3+} ions are created at the time of cooling procedure, because of Oxygen ingestion. Thus the electron trade among the ions of similar component is in charge of the change of ac conductivity.

6.2.2 Temperature dependence

A plot of ln σ_{ac} vs. $\frac{1}{T}$ for x= 0.0, 0.1 and 0.2 are delineated in Fig. 6.4(a)-(c). It is noticed that the conductivity raises with temperature, demonstrating semiconducting character of the present sample. Consequently, CZMO ferrite is portrayed as a magnetic semiconductor. Fig. 6.4(d) demonstrates the fitted straight line (solid line) for x=0.2 at 100 kHz relating to Arrhenius condition. It is obviously found in Fig. 6.4(d) that the change of slope of the straight line happens at a specific temperature, which is known as the Curie temperature (T_C) of the material.

At higher temperature, i.e., in paramagnetic domain the conductivity is about free of frequency on the grounds that the electron conduction in this domain relates to band

conduction model while at lower temperature, i.e., in ferrimagnetic domain the conduction relates to hopping conduction mechanism. Accordingly, the ac conduction is temperature as well as frequency reliant [123].

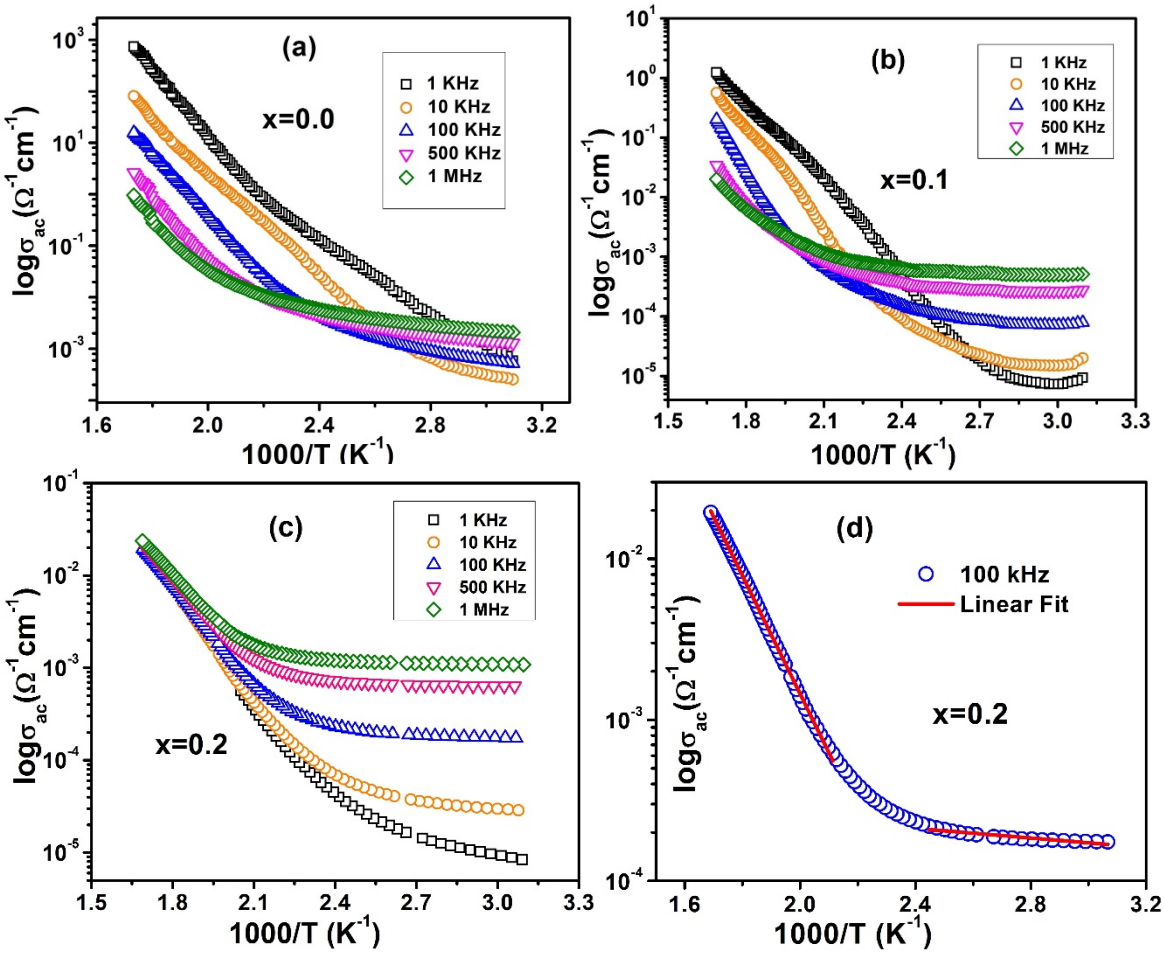

Fig. 6.4. (a)-(c) The variation of σ_{ac} with $\frac{1}{T}$ at different frequencies for Mo doped Co-Zn ferrite. (d) Fitted straight line plot according to Arrhenius law at 100 KHz.

The activation energies in paramagnetic as well as ferrimagnetic domain may be calculated from the slope of the straight line utilizing the Arrhenius equation

$$\sigma_{ac} = \sigma_0 \exp(^{-E_a}/_{k_B T}) \qquad (6.7)$$

where σ_0 reresents the pre-factor and the activation energy is E_a. The estimated activation energies of the considerable number of samples at various frequency for paramagnetic as well as ferrimagnetic domain are delineated in Table 6.2.

Table 6.2. List of calculated activation energy E_p and E_f at different frequencies.

X	E_p in eV (High temperature region)					E_f in eV (Low temperature region)				
	1kHz	**10 kHz**	**100 kHz**	**500 kHz**	**1 MHz**	**1kHz**	**10 kHz**	**100 kHz**	**500 kHz**	**1 MHz**
0.0	1.29	0.97	1.19	1.18	1.08	0.69	0.29	0.24	0.15	0.10
0.1	0.41	0.57	0.60	0.49	0.37	0.021	0.015	0.015	0.014	0.01
0.2	0.30	0.34	0.31	0.27	0.26	0.056	0.026	0.01	0.004	0.005

The activation energy in the paramagnetic domain (E_p) is higher than that in the ferrimagnetic domains (E_f) because of the way that the paramagnetic phase is a disordered phase compare to ordered ferrimagnetic phase. Thusly, the charge carriers in the paramagnetic phase required more energy to hop between the neighboring sites. This outcome is in great concurrence with the model proposed by Irkhin and Turov [226].

6.3 Magnetization study

Mo substituted Co-Zn ferrites are in type of ferrimagnetic materials having inverse spinel crystal structure. Detail magnetic estimations M (H,T) uncover the sort of magnetic ordering exists in the material. Fig. 6.5 demonstrates the variation of magnetization with temperature for x=0.0 and x=0.2 samples proposing that the magnetization increments

marginally with temperature, accomplishes a most extreme and begins strongly diminishing at a specific temperature which describes the Curie temperature (T_C) (Ferrimagnetic → Paramagnetic) of the material after which the material turned into paramagnetic. The inset of the Fig. 6.5 depicts dM/dT vs. T curves for each sample which unmistakably demonstrate sharp crest in dM/dT where all M(T) curve has a state of enunciation. This relates to T_C of the present samples.

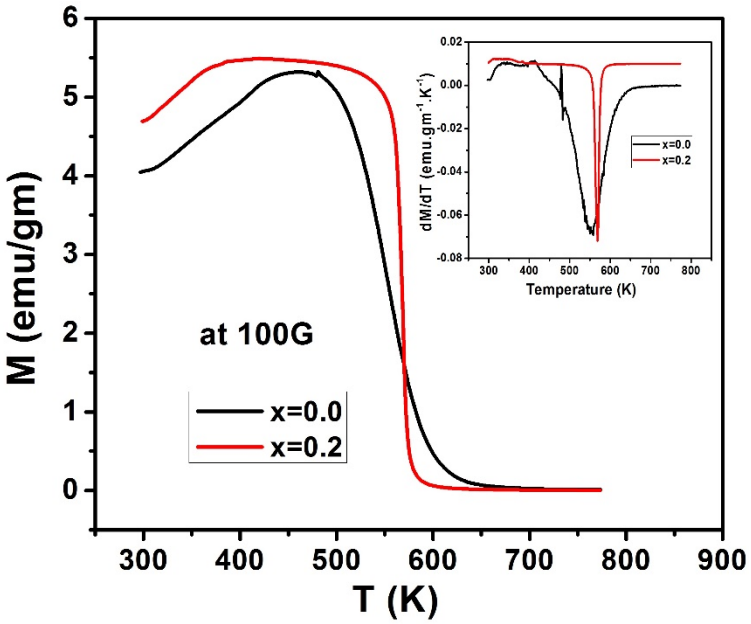

Fig. 6.5. Variation of Magnetization (M) with absolute temperature (T) of CZMO (x=0.0 and 0.2). The inset represents the derivative of magnetization vs. temperature (dM/dT vs. T) plots of both x=0.0 and 0.2 samples.

The observed Curie temperature for x=0.0 sample is about ~556 K and for x=0.2 sample it's appeared to be at ~570 K. The estimation of T_C and saturation magnetization is observed to be enhanced due to Mo substitution in Co-Zn ferrite. Additionally, on account of x=0.2 sample, there is a sharp plunge under T=380 K which propose another magnetic transition conceivably exist in high Mo doping concentration at bring down temperature.

Be that as it may, facilitate estimations are need to investigate the idea of magnetic ordering underneath the 2nd magnetic transition for x=0.2 sample.

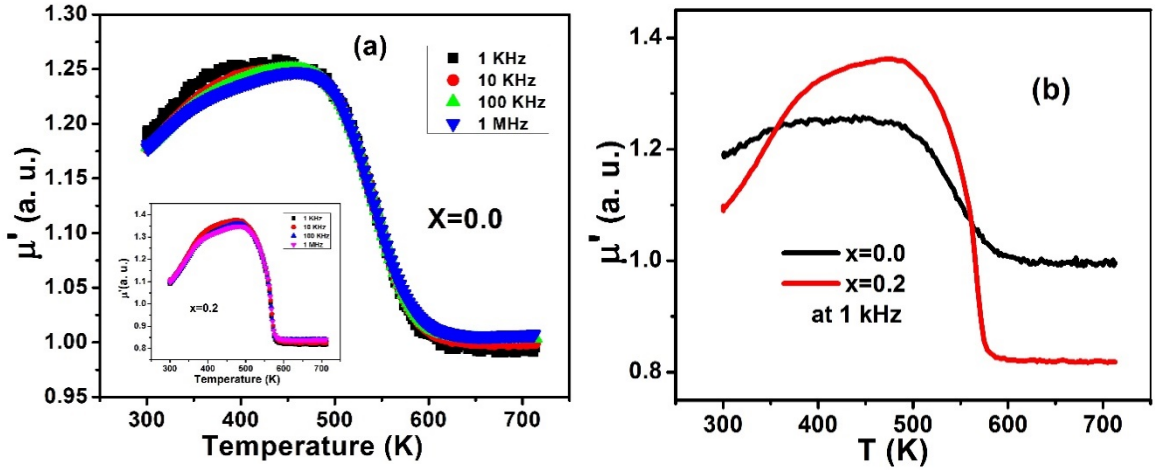

Fig. 6.6. (a)Temperature dependence of real permeability at different frequencies for x=0.0 and inset shows the same for x=0.2. (b) μ' vs. T plot for x=0.0 and 0.2 at 1kHz.

The temperature reliance of real part of permeability ($\mu = \mu' + i\mu'' = \mu_0(1 + \chi)$) at various frequency for x=0.0 and 0.2 is presented in Fig. 6.6(a) and its inset, separately. The curves (Fig. 6.6(b)) take after the comparative patterns like the M-T plots (Fig. 6.5). Additionally, the Curie temperature for both x=0.0 and 0.2 is observed to be similar as saw in M-T plots.